

Supplementary Materials for

**Nearest-Neighbour Nanocrystal Bonding Dictates Framework Stability  
or Collapse in Colloidal Nanocrystal Frameworks**

Teresa E. Williams, Daniela Ushizima, Chenhui Zhu, André Anders, Delia J. Milliron, Brett A. Helms\*

\*correspondence to: [bahelms@lbl.gov](mailto:bahelms@lbl.gov)

This PDF includes:

**Materials and Methods**  
**Figures S1–S16**  
**Tables S1–S5**  
**Notes on DiameterJ analysis**  
**References**

**Materials and Methods.**

Ethanol (EtOH, anhydrous,  $\geq 99.5\%$ ), toluene (anhydrous, 99.8%) and *N,N*-dimethylformamide (DMF, anhydrous, 99.8%) were obtained from Sigma-Aldrich and passed through a 0.2  $\mu\text{m}$  PTFE (EtOH, toluene) or PVDF (DMF) syringe-tip filter (Whatman) prior to use. Nitrosyl tetrafluoroborate was obtained from Sigma-Aldrich and used as received.  $\langle 100 \rangle$  Si wafers (single-sided polished) were obtained from Silicon Quest. Thermogravimetric analysis (TGA) was carried out using a TA Instruments Q5000IR TGA-MS. Transmission electron microscopy (TEM) images were taken with a JEOL 2100F at an acceleration voltage of 200 kV; samples were prepared by dropping a dilute solution onto an ultrathin carbon film supported by a lacey carbon film on a 400 mesh Cu grid (Ted Pella), then drying in air. Scanning electron microscope (SEM) images were taken with a Zeiss Gemini Ultra-55, equipped with in-lens and secondary electron detectors, at an acceleration voltage of 5 kV. X-ray Diffraction (XRD) was performed on a Bruker Gaddsd8 Diffractometer with a Co-K $\alpha$  source operating at 45 kV and 30 mA. Grazing Incidence Small Angle X-ray Scattering (GISAXS) experiments were carried out at Beamline 7.3.3 at the Advanced Light Source at Lawrence Berkeley National Laboratory, using an incident angle of 0.16°, a wavelength of 1.24 Å (10

keV), and a sample to detector distance of 3.8 m. Images were recorded on a Pilatus 2M detector (pixel size: 172  $\mu\text{m}$  x 172  $\mu\text{m}$ ) from Dectris. Image processing was carried out in Igor Pro using the SAS 2D plugin for data reduction.<sup>1</sup> Total porosity for all films was determined by Rutherford Backscattering Spectroscopy (RBS) using a 5SDH Pelletron tandem accelerator (National Electrostatics Corporation).

### Synthesis of ligand-stripped tin-doped indium oxide (ITO) nanocrystals

ITO NCs were prepared and purified as described previously.<sup>2</sup> Ligand stripping was carried as described previously<sup>3</sup> in an oxygen- and water-free glove box using  $\text{NOBF}_4$ . NCs were precipitated three times with toluene and redispersed in DMF at a concentration of 11.3 wt % (TGA). ImageJ software was used to determine the distribution of nanocrystal size (Figure S1) from a series of TEM images ( $n = 276$ ,  $d = 5.3 \text{ nm} \pm 0.7 \text{ nm}$ ).

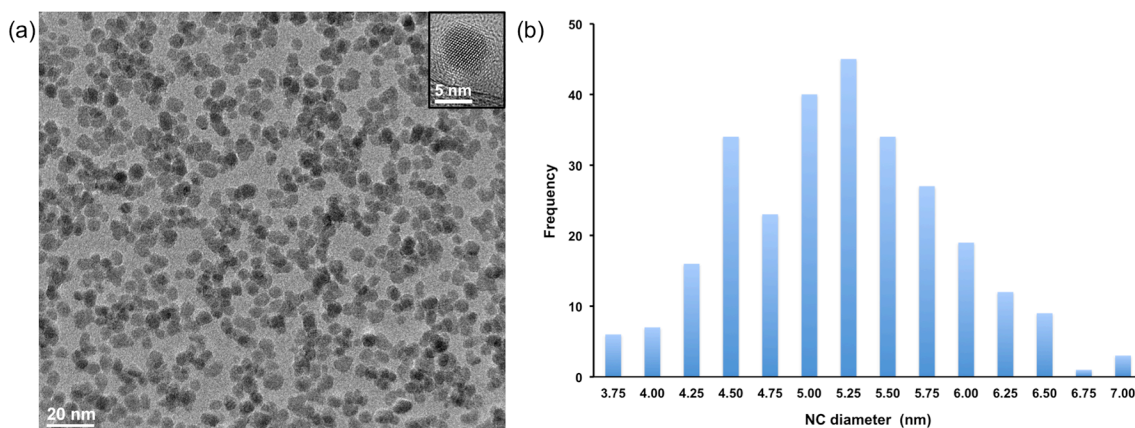


**Figure S1.** (a) TEM image of ligand-stripped ITO nanocrystals and (b) histogram for size-distribution analysis.

### Assembly of PS-*b*-PDMA Micelles

PS-*b*-PDMA copolymers were prepared as described previously.<sup>4</sup> To assemble the micelles, PS-*b*-PDMA was dissolved in DMF, then EtOH was added drop-wise to make a 25  $\text{mg mL}^{-1}$  BCP solution in 8:2 v/v EtOH/DMF. ImageJ software was used to determine the distribution of micelle sizes from a series of TEM images (Figs. S2 & S3).

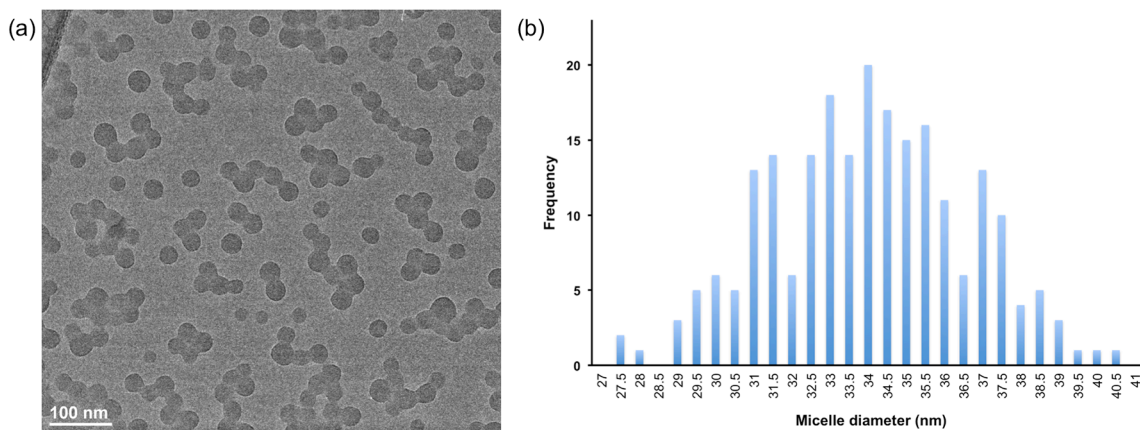


**Figure S2.** (a) TEM image of PS<sub>60k</sub>-*b*-PDMA<sub>20k</sub> micelles and (b) histogram for size-distribution analysis ( $n = 248$ ,  $d = 34.4 \text{ nm} \pm 2.3 \text{ nm}$ ).

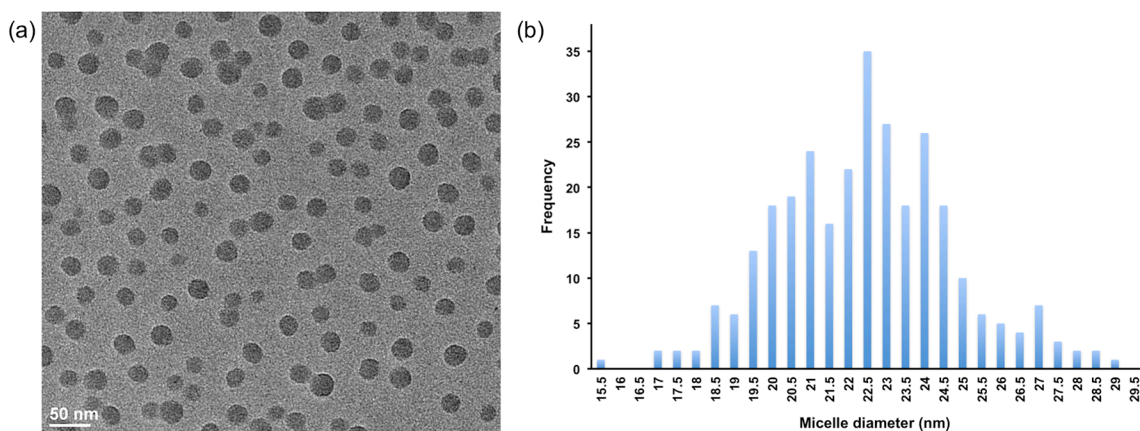


**Figure S3.** (a) TEM image of PS<sub>20k</sub>-*b*-PDMA<sub>20k</sub> micelles and (b) histogram for size-distribution analysis ( $n = 296$ ,  $d = 22.7 \text{ nm} \pm 2.3 \text{ nm}$ ).

### Assembly of BCP micelle-ITO NC binary colloidal assemblies

Assemblies were prepared by adding the appropriate weight of ITO NC solution in DMF to a stirring solution of BCP micelles (Table S1). Samples were equilibrated overnight at ambient temperature.

**Table S1.** Ratio of ITO NC and BCP for preparation of binary colloidal assemblies.

Sample	NC wt (mg/mL)	BCP wt (mg/mL)	BCP% w/w	NC% w/w
1	183.33	25	12	88
2	100.00	25	20	80
3	64.28	25	28	72
4	44.44	25	36	64
5	31.82	25	44	56
6	23.07	25	52	48
7	16.67	25	60	40

### Preparation of mesoporous ITO colloidal nanocrystal frameworks

Substrates were prepared by spin coating 50  $\mu\text{L}$  of BCP-NC solution onto a 2x2  $\text{cm}^2$  Si wafer with a 3 s ramp to 800 rpm, then held at 800 rpm for 3 min. Mesoporosity was revealed following annealing in air with a 3 h ramp from rt to 550  $^\circ\text{C}$ , then held at 550  $^\circ\text{C}$  for 1.5 h. X-ray diffraction confirmed the crystal structure of ITO NCs in the resulting mesoporous framework (Figure S4).

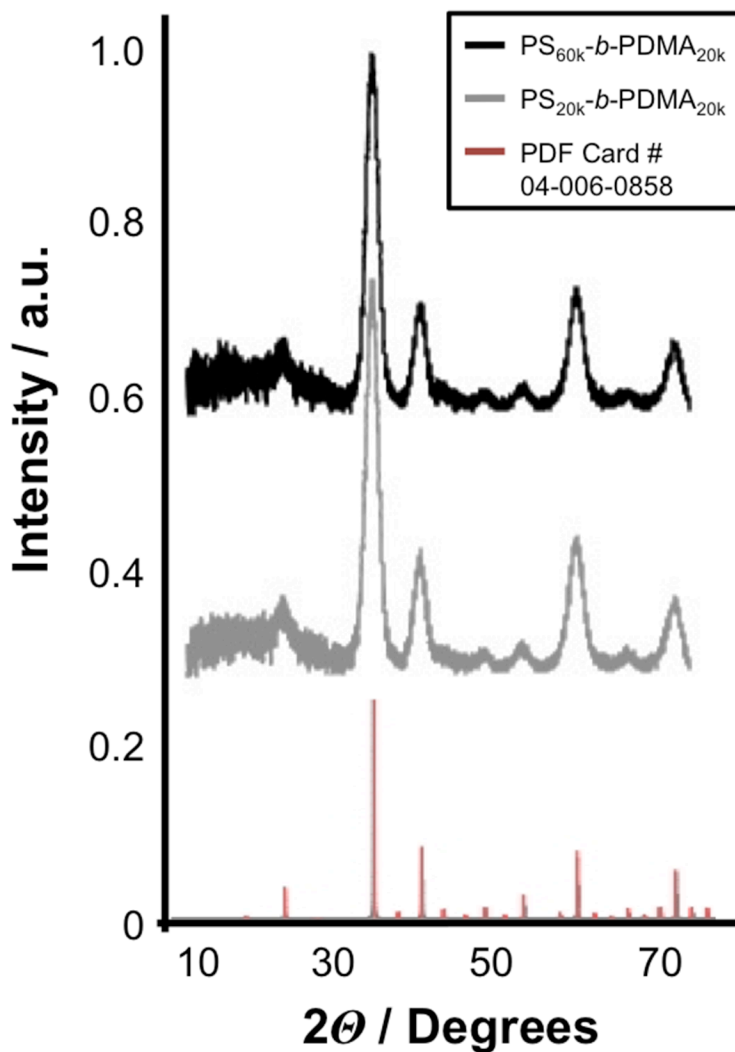


**Figure S4.** X-ray diffraction characterization of mesoporous ITO nanocrystal framework. Overlay of traces of diffraction patterns for frameworks generated from 52% w/w PS<sub>60k</sub>-b-PDMA<sub>20k</sub> (black trace) or PS<sub>20k</sub>-b-PDMA<sub>20k</sub> (grey trace) with JCPDS standard diffraction pattern for tin-doped indium oxide NCs (red trace). Spectra are offset for clarity.

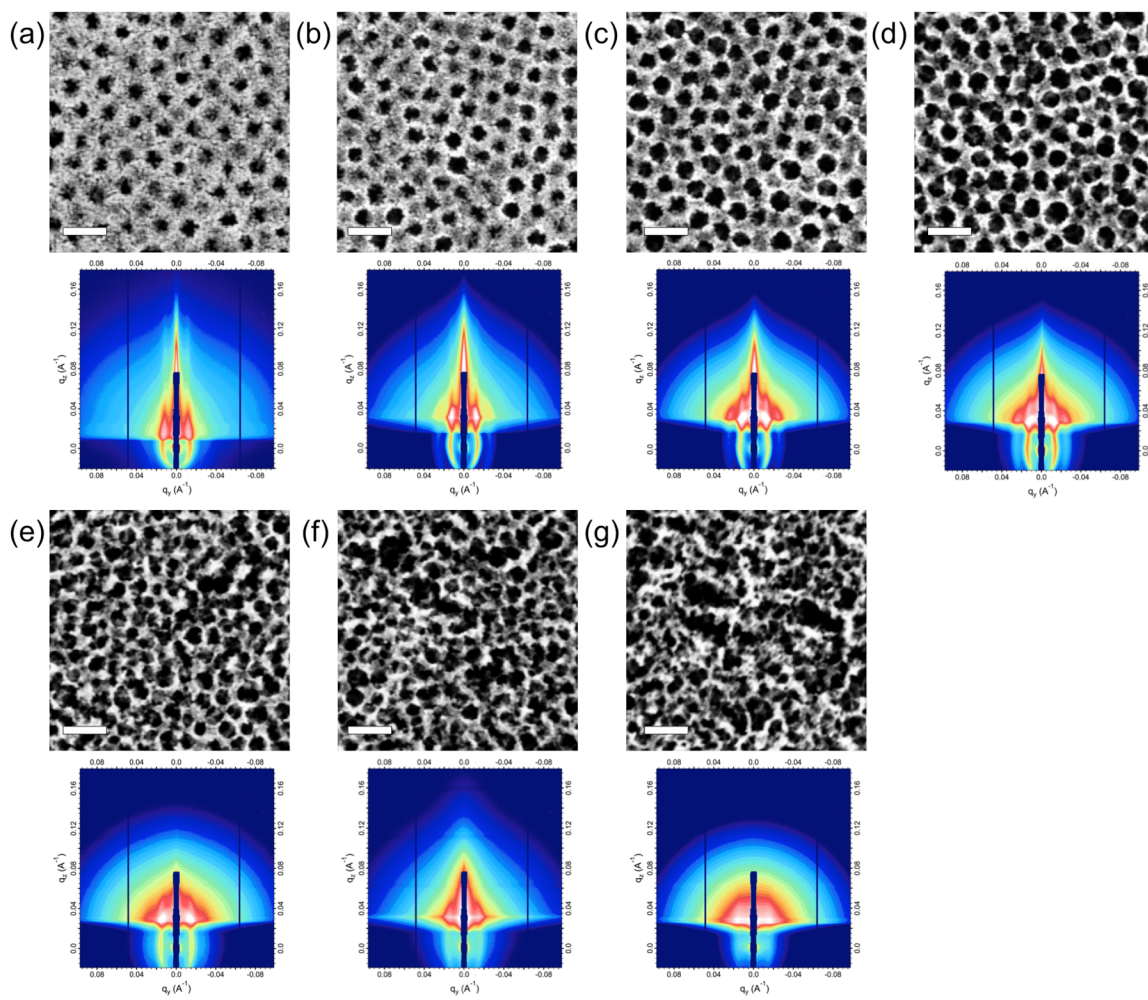


**Figure S5.** Evolution of film architecture as a function of BCP loading, as evidenced by top-down SEM and GISAXS, for  $\text{PS}_{60\text{k}}\text{-}b\text{-PDMA}_{20\text{k}}$  at BCP loadings of: (a) 12%; (b) 20%; (c) 28%; (d) 36%; (e) 44%; (f) 52%; (g) 60% *w/w*. Scale bar = 100 nm.

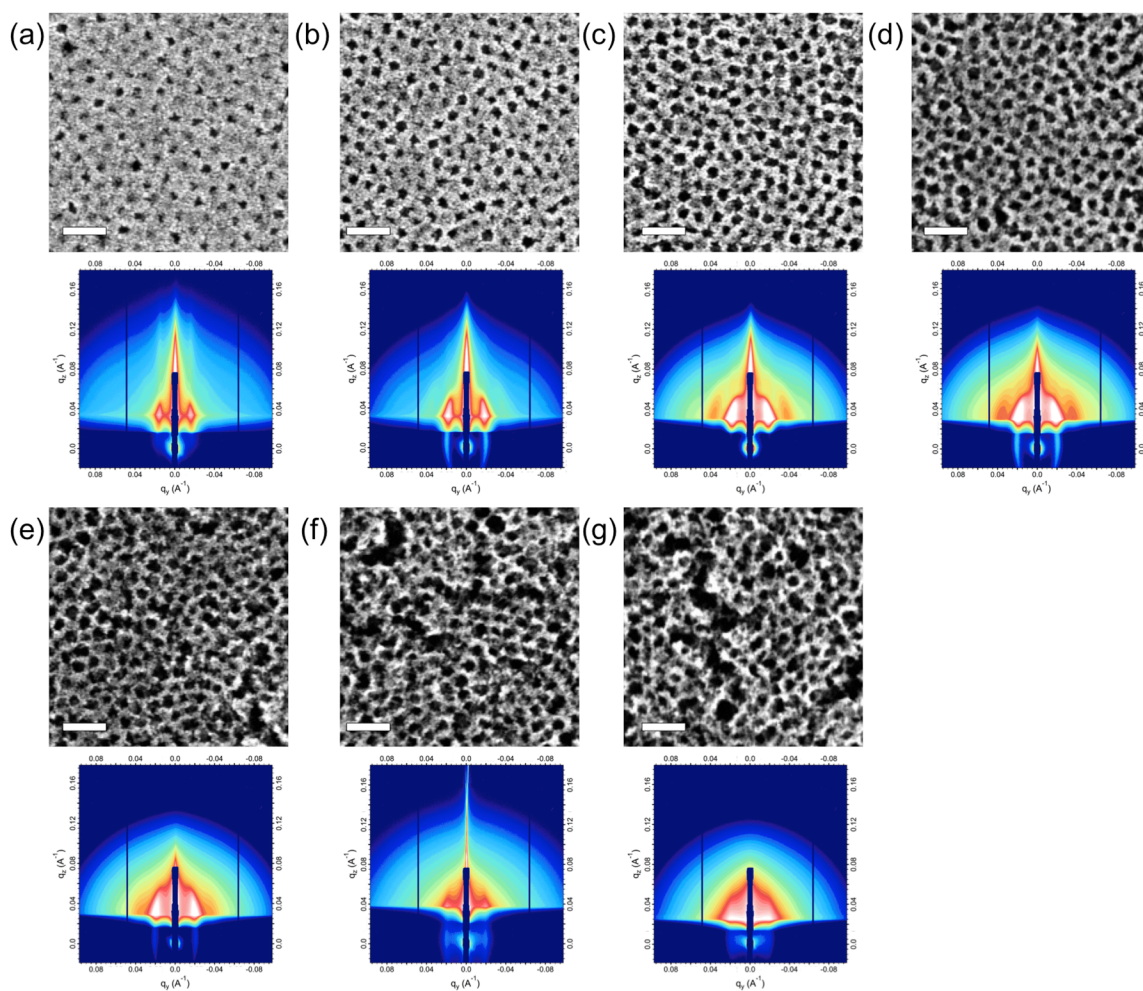


**Figure S6.** Evolution of film architecture as a function of BCP loading, as evidenced by top-down SEM and GISAXS, for  $\text{PS}_{20k}\text{-}b\text{-PDMA}_{20k}$  at BCP loadings of: (a) 12%; (b) 20%; (c) 28%; (d) 36%; (e) 44%; (f) 52%; (g) 60% *w/w*. Scale bar = 100 nm.

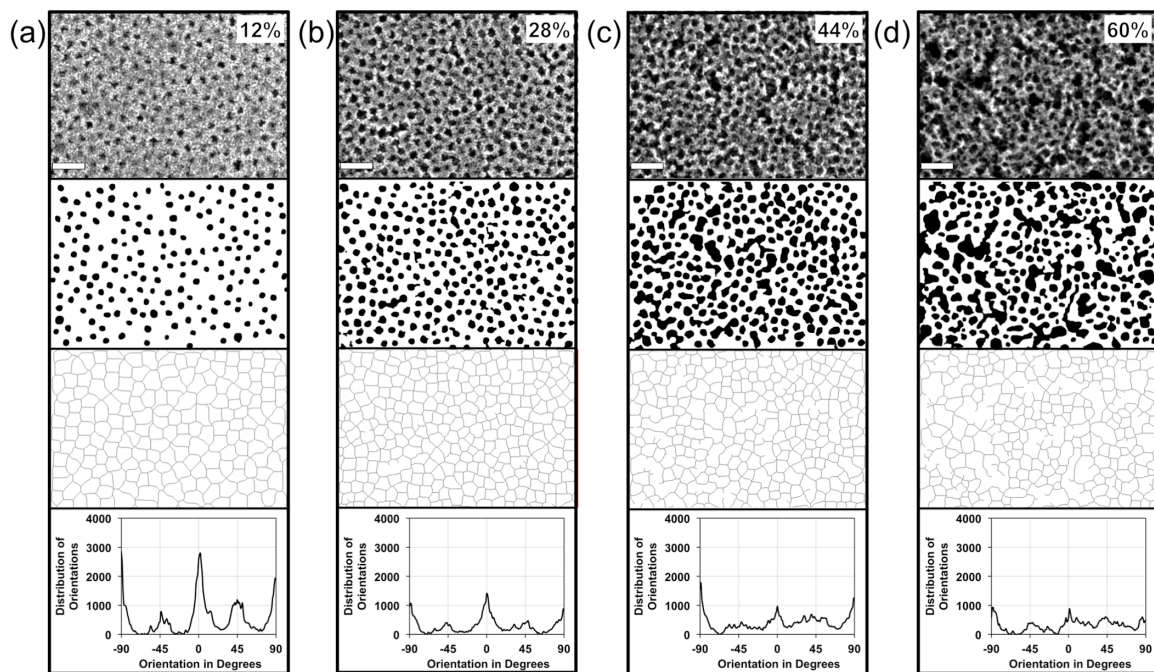


**Figure S7.** Top-down SEM, binary segmentation, Voronoi diagram, and orientation analysis for films assembled using PS<sub>20k</sub>-*b*-PDMA<sub>20k</sub> at a BCP loading of: (a) 12%; (b) 28%; (c) 44%; or (d) 60% w/w. Scale bar = 100 nm.

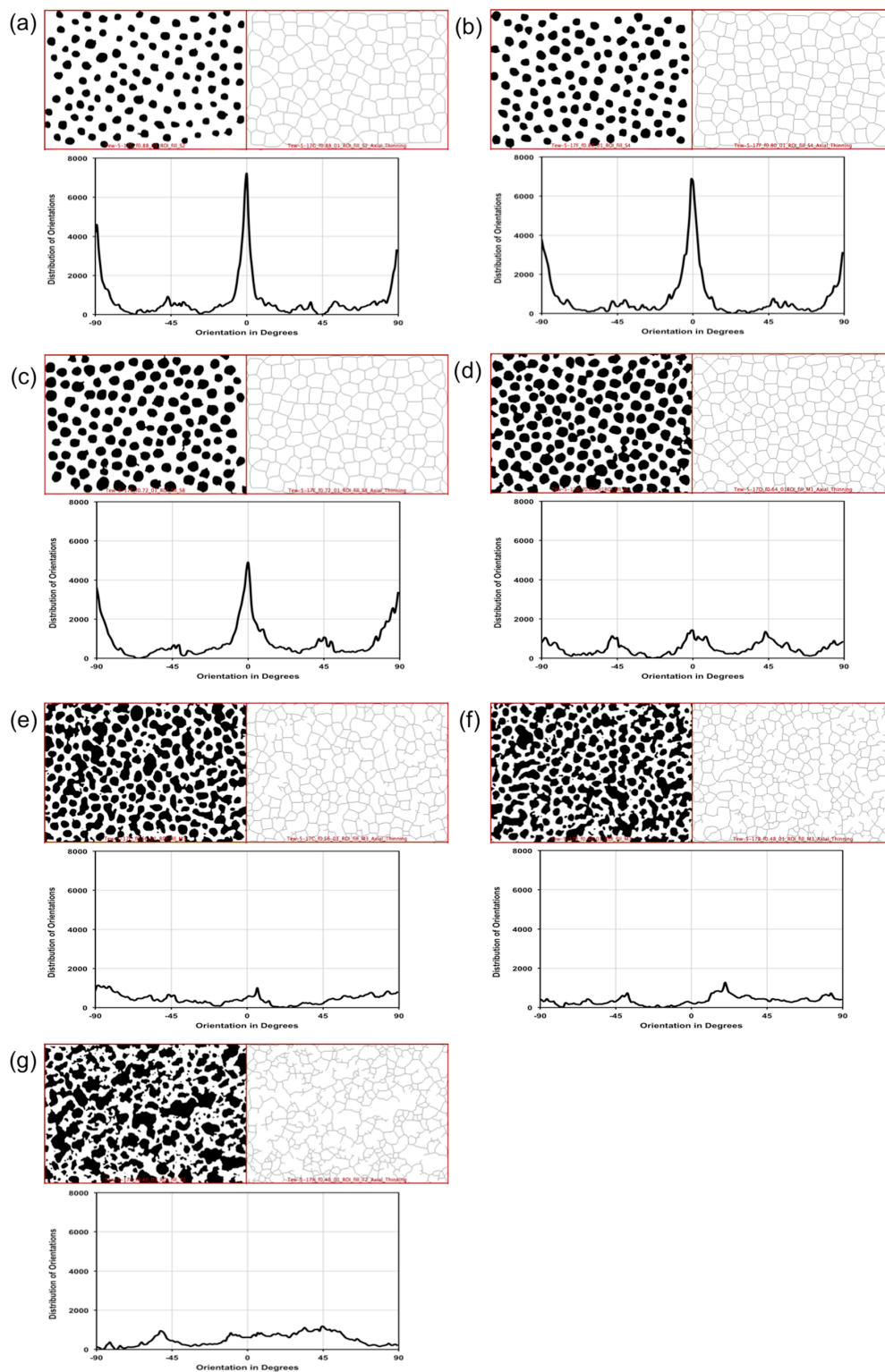


**Figure S8.** Binary segmentation, Voronoi diagram, and orientation analysis for films assembled with PS<sub>60k</sub>-*b*-PDMA<sub>20k</sub> at all BCP loadings: (a) 12%; (b) 20%; (c) 28%; (d) 36%; (e) 44%; (f) 52%; (g) 60% w/w.

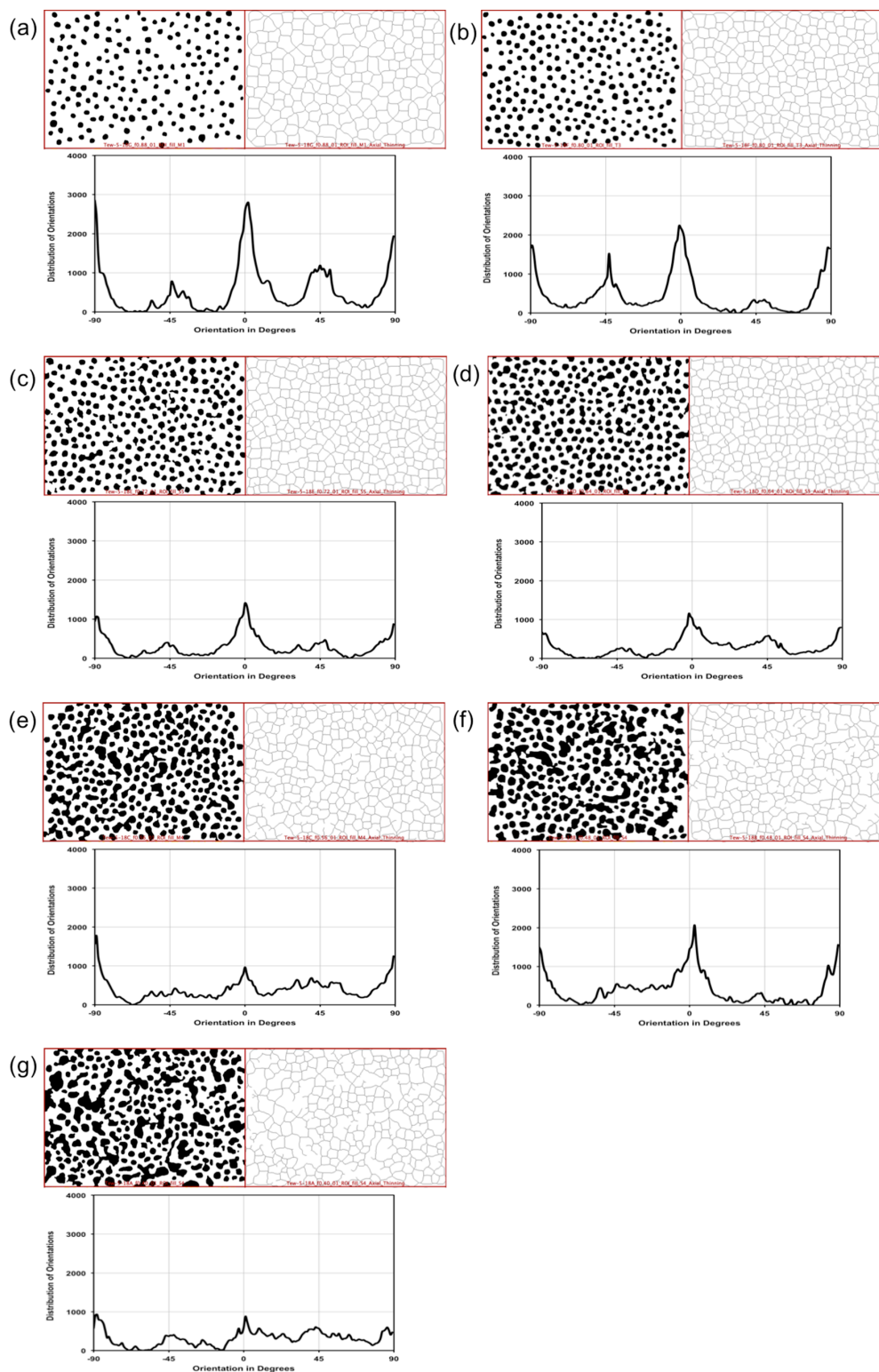


**Figure S9.** Binary segmentation, Voronoi diagram, and orientation analysis for films assembled with PS<sub>20k</sub>-*b*-PDMA<sub>20k</sub> at all BCP loadings: (a) 12%; (b) 20%; (c) 28%; (d) 36%; (e) 44%; (f) 52%; (g) 60% w/w.

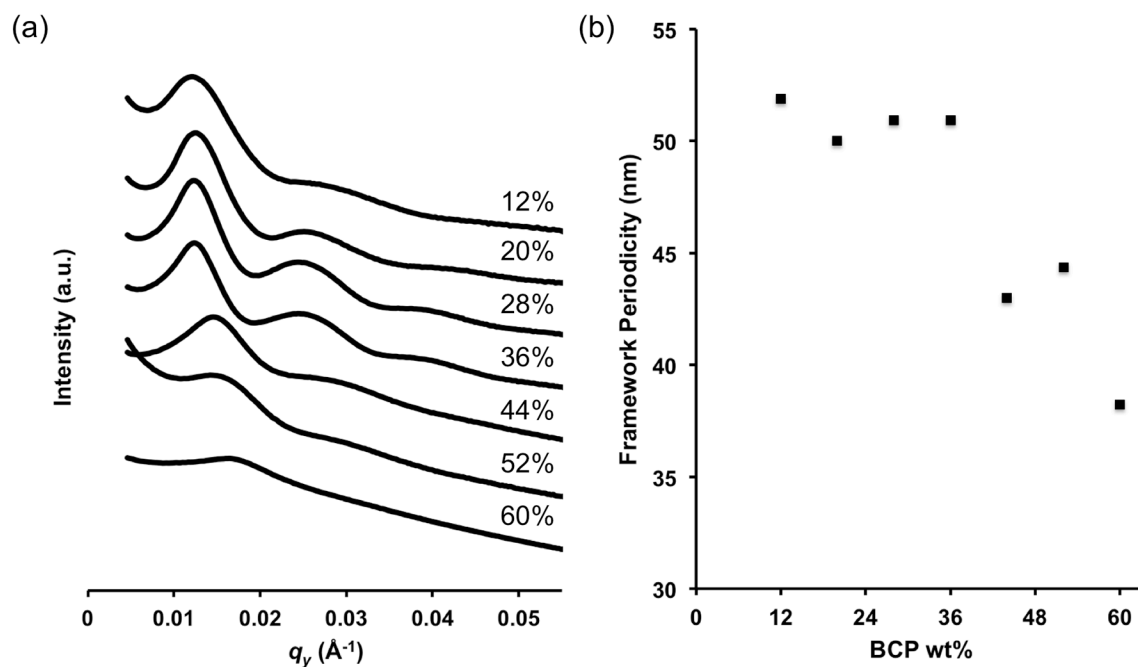


**Figure S10.** (a) Horizontal line cuts from GISAXS scattering patterns, with BCP loading indicated on each trace; (b) plot of framework periodicity as a function of BCP loading for films assembled with PS<sub>60k</sub>-b-PDMA<sub>20k</sub> micelles.

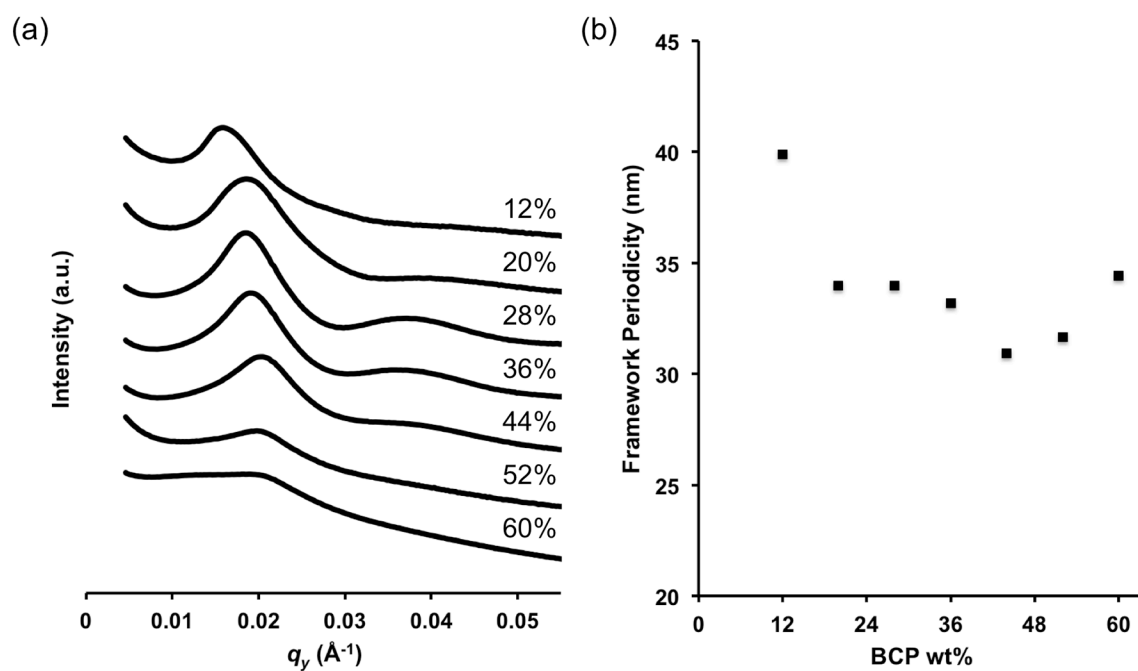


**Figure S11.** (a) Horizontal line cuts from GISAXS scattering patterns, with BCP loading indicated on each trace; (b) plot of framework periodicity as a function of BCP loading for films assembled with PS<sub>20k</sub>-b-PDMA<sub>20k</sub> micelles.

**Table S2:** Pore area and circularity, and their standard deviation (SD), from ImageJ analysis on binary, top-down SEM images.

BCP % w/w	PS <sub>60k</sub> - <i>b</i> -PDMA <sub>20k</sub>				PS <sub>20k</sub> - <i>b</i> -PDMA <sub>20k</sub>			
	Pore area (nm <sup>2</sup> )	SD (nm <sup>2</sup> )	Pore circularity	SD	Pore area (nm <sup>2</sup> )	SD (nm <sup>2</sup> )	Pore circularity	SD
12	677.374	148.845	0.900	0.032	292.868	68.303	0.917	0.022
20	776.238	136.052	0.897	0.030	300.104	77.947	0.920	0.016
28	1058.759	248.455	0.872	0.076	374.571	164.670	0.848	0.121
36	1139.791	601.252	0.838	0.134	416.420	224.492	0.839	0.126
44	1101.71	1176.40	0.76	0.20	624.36	528.63	0.80	0.17
52	941.39	1270.09	0.74	0.22	801.76	1013.23	0.77	0.20
60	919.45	2197.30	0.71	0.24	723.60	913.82	0.78	0.19

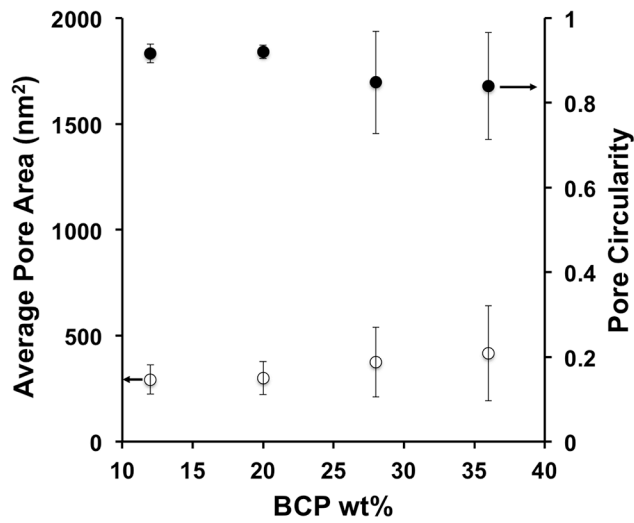


**Figure S12.** Average pore area (open circles) and pore circularity (filled circles) vs. BCP loading for CNFs assembled with PS<sub>20k</sub>-*b*-PDMA<sub>20k</sub>. Pore diameters were: 19 nm at 12%, 19 nm at 20%, 22 nm at 28%, and 23 nm at 36% BCP loading w/w.

**Table S3.** Film thickness measurements for all samples as analyzed by ImageJ from cross-sectional SEM images.

BCP wt%	PS <sub>60k</sub> - <i>b</i> -PDMA <sub>20k</sub>		PS <sub>20k</sub> - <i>b</i> -PDMA <sub>20k</sub>	
	Thickness (nm)	SD (nm)	Thickness (nm)	SD (nm)
12	425.10	5.29	437.26	10.93
20	443.05	4.87	410.48	5.97
28	376.59	8.57	403.20	3.28
36	355.37	5.19	356.31	5.63
44	281.86	3.72	363.06	5.41
52	297.34	8.46	264.33	5.11
60	242.61	4.27	291.02	4.32

**Table S4.** Determination of  $f_{NC}$  for all films from fitting RBS data using SIMNRA software.

	PS <sub>60k</sub> - <i>b</i> -PDMA <sub>20k</sub>	PS <sub>20k</sub> - <i>b</i> -PDMA <sub>20k</sub>
BCP wt%	$f_{NC}$	$f_{NC}$
12	0.56	0.55
20	0.395	0.455
28	0.38	0.375
36	0.282	0.375
44	0.2685	0.3
52	0.1975	0.17
60	0.265	0.33

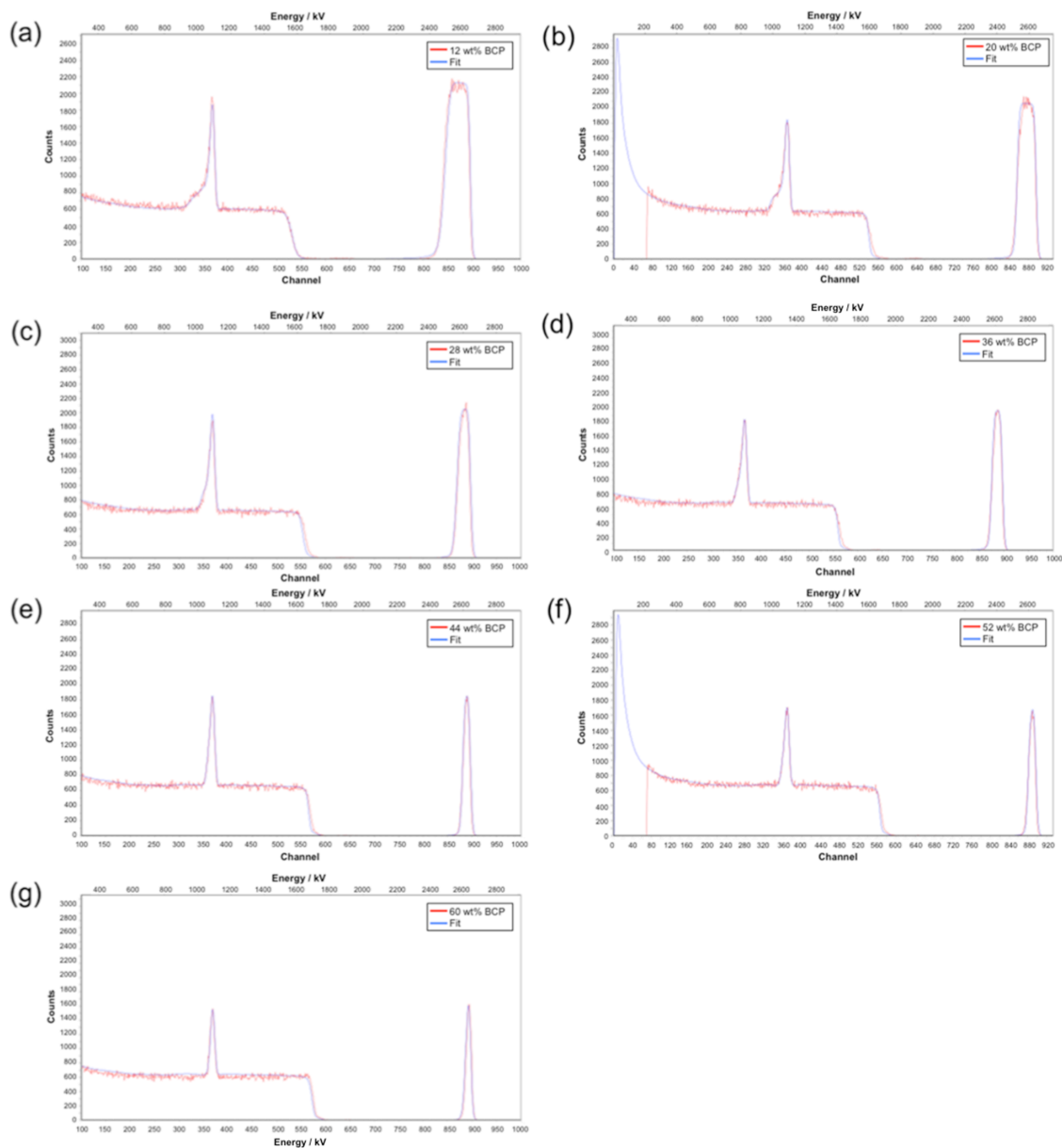


**Figure S13.** Sample data (red trace) and fits (blue trace) from RBS measurements for films assembled using PS<sub>60k</sub>-*b*-PDMA<sub>20k</sub> micelles at variable loadings of: (a) 12%; (b) 20%; (c) 28%; (d) 36%; (e) 44%; (f) 52%; (g) 60% w/w.

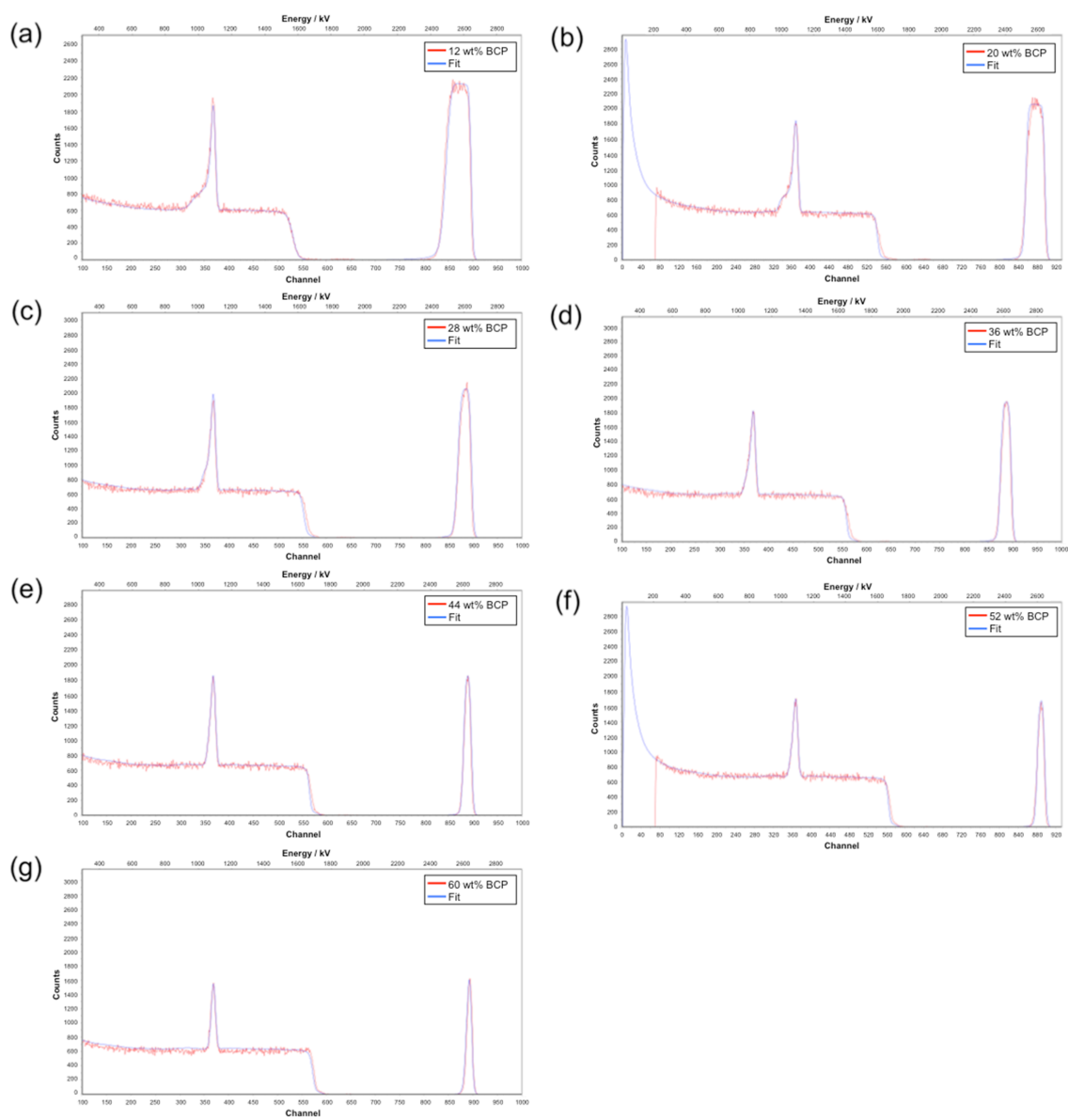


**Figure S14.** Sample data (red trace) and fits (blue trace) from RBS measurements for films assembled using PS<sub>20k</sub>-*b*-PDMA<sub>20k</sub> micelles at variable loadings of: (a) 12%; (b) 20%; (c) 28%; (d) 36%; (e) 44%; (f) 52%; (g) 60% *w/w*.

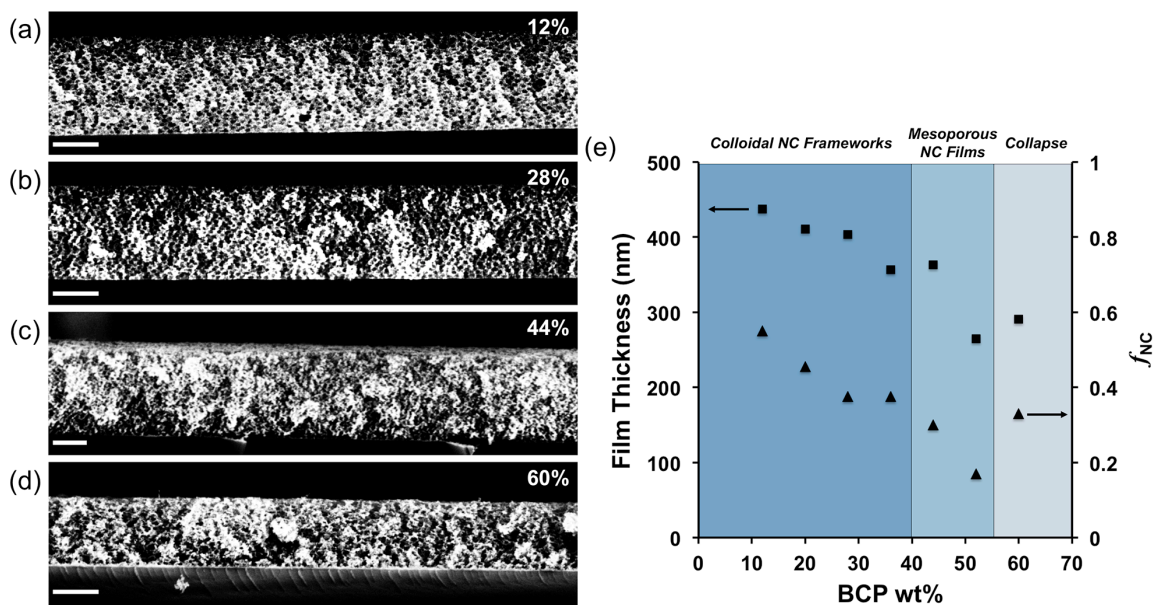


**Figure S15.** Cross-sectional SEM images for films assembled using PS<sub>20k</sub>-*b*-PDMA<sub>20k</sub> at a BCP loading of: (a) 12%; (b) 28%; (c) 44%; or (d) 60% w/w; (e) Film thickness (squares) &  $f_{NC}$  (triangles) vs. BCP loading. Scale bar = 200 nm.

**Table S5.** Load-bearing segment widths from DiameterJ analysis for all films.

BCP% w/w	PS <sub>60k</sub> - <i>b</i> -PDMA <sub>20k</sub>		PS <sub>20k</sub> - <i>b</i> -PDMA <sub>20k</sub>	
	Width (nm)	SD (nm)	Width (nm)	SD (nm)
12	26.04	7.13	22.59	5.60
20	21.89	6.67	17.34	5.08
28	16.18	5.59	14.31	4.28
36	12.82	4.50	12.48	4.00
44	10.57	3.97	11.23	4.15
52	10.09	4.21	10.88	4.08
60	9.58	4.23	11.20	4.56

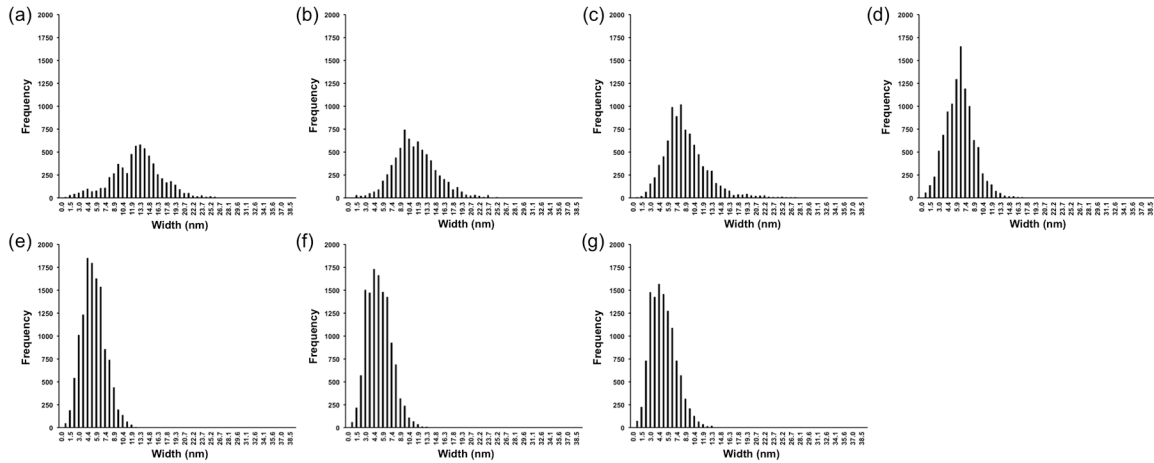


**Figure S16.** Distribution of segment widths for films assembled with PS<sub>60k</sub>-*b*-PDMA<sub>20k</sub> micelles at BCP loadings of: (a) 12%; (b) 20%; (c) 28%; (d) 36%; (e) 44%; (f) 52%; (g) 60% w/w.

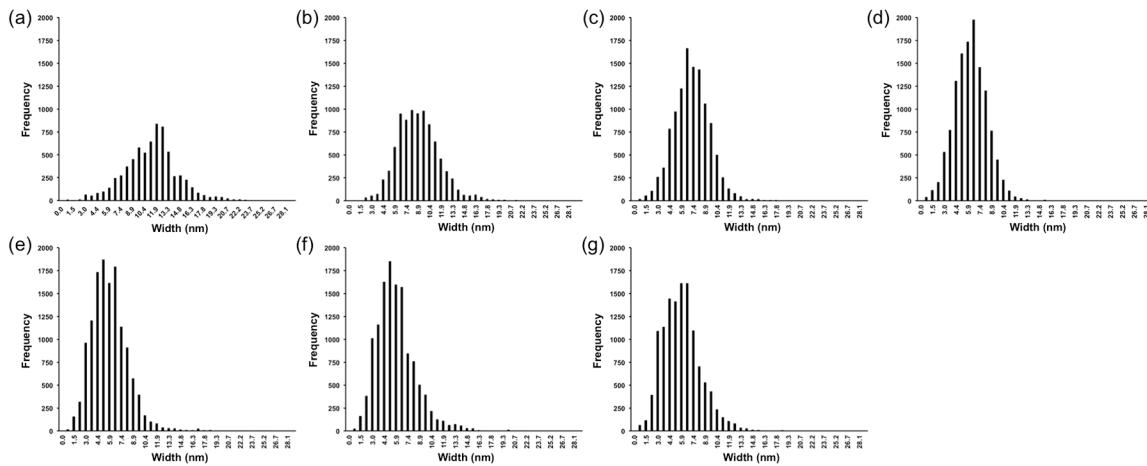


**Figure S17.** Distribution of segment widths for films assembled with PS<sub>20k</sub>-*b*-PDMA<sub>20k</sub> micelles at BCP loadings of: (a) 12%; (b) 20%; (c) 28%; (d) 36%; (e) 44%; (f) 52%; (g) 60% w/w.

### DiameterJ Analysis

<http://imagej.net/DiameterJ>

DiameterJ is an open source plugin for ImageJ developed at NIST (National Institutes of Standards and Technology) and is a validated nanofiber diameter characterization tool. It is bundled with OrientationJ, for analysis of ‘fiber’ orientation within an image, and also the ‘Analyze Particles’ function to analyse pore space within scaffolds and produce summary statistics for pores. DiameterJ is a two-step process of image analysis: (1) image segmentation into a binary image; (2) analysis of segmented image.

Though our films consist of interconnected frameworks comprised of colloidal nanocrystals rather than individual nanofibers, the analyses are made on binary images, which have been segmented for matter (framework) and void spaces (pores); this makes the calculations applicable for our desired analyses.

For orientation analysis: this method is based upon Fourier spectrum analysis using a Gaussian window of 7 pixels. The subsequent frequency histogram of orientations is generated. Analyses were also carried out, for comparison, using both cubic spline and Gaussian gradients, with the Gaussian window ranging from 1–7 pixels; results were consistent across these methods.

For pore size analysis: the algorithm looks for discrete clusters of black pixels, which indicate pores in our samples rather than individual particles, counts the number of pixels in each cluster, and reports their area. Clusters on the edges of the image are excluded. Reports of pore area and standard deviation, and pore circularity and standard deviation, are included.

For segment width analysis: binary, top-down SEM images were analysed to find the centerlines of the framework segments, then the width was determined by examining every pixel along the framework's axis to produce a histogram of the framework widths. Included are summary statistics such as mean segment width and standard deviation.

## References.

1. J. Ilavsky, *J. Appl. Cryst.*, 2012, **45**, 324.
2. S. D. Lounis, E. L. Runnerstrom, A. Bergerud, D. Nordlund, and D. J. Milliron, *J. Am. Chem. Soc.*, 2014, **136**, 7110.
3. A. Dong, X. Ye, J. Chen, Y. Kang, T. Gordon, J. M. Kikkawa, and C. B. Murray, *J. Am. Chem. Soc.*, 2011, **133**, 998.
4. R. Buonsanti, T. E. Pick, N. Krins, T. J. Richardson, B. A. Helms, and D. J. Milliron, *Nano Lett.*, 2012, **12**, 3872.